Proceedings of the ASME 2023 42th International Conference on Ocean, Offshore and Arctic Engineering
OMAE2023
June 11-16, 2023, Melbourne, Australia

OMAE2023-105065

WAVE-CURRENT INTERACTION WITH FLOATING OBJECTS WITH SQUARE AND CIRCULAR WATERPLANE AREAS

Azin Lamei
Civil Engineering Department
University of Dundee
Dundee, DD1 4HN, UK
Email: alamei@dundee.ac.uk

Shuijin Li
Civil Engineering Department
University of Dundee
Dundee, DD1 4HN, UK
Email: skli@dundee.ac.uk

Masoud Hayatdavoodi
Civil Engineering Department
University of Dundee
Dundee, DD1 4HN, UK

& College of Shipbuilding
Engineering
Harbin Engineering University
Harbin, China
Email: mhayatdavoodi@dundee.ac.uk

H. Ronald Riggs
Civil and Environmental
Engineering Department
University of Hawaii at Manoa
Honolulu, HI 96822, USA
Email: riggs@hawaii.edu

ABSTRACT

Floating pontoons of different shapes are used commonly as the base of floating offshore wind turbines, and as wave breakers to mitigate severity of incoming waves. The pontoons are typically attached to catenary mooring lines and often operate in areas subject to large environmental loads, including waves, current and wind. It is of interest to analyse the wave-current interaction with pontoons of various shapes, and assess the effect of the shape of the body, wave-current direction, and the mooring lines on the loads and responses. In this study, attention is confined to wave-current interaction with floating objects with square and circular waterplane areas. A range of wave conditions is considered and the solution is obtained by the Green-function method for small forward speeds within the context of the linear wave diffraction theory. Results include the wave-current-induced forces, and the motion of the body. Both conditions of freely floating and objects attached to catenary mooring lines are considered, subject to various wave-current directions. Computations are carried out in frequency domain and results of the two models are compared with each other. Discussion is provided on the effect of the mooring lines and the wave-current direction on the responses of the objects.

Keywords: Floating offshore structure, Wave-current-structure interaction, small forward speed Green function, linear wave diffraction theory.

1 Introduction

Study of wave and current interaction with freely floating or moored structures is of great importance in oil and gas industry, ships and submarines and offshore renewable

Copyright © 2023 by ASME

energy converters, among others. Knowledge on responses of a floating structure to various wave conditions and combined waves and current loads is essential for its design, understanding of its optimum performance and planning its operation and maintenance procedure.

Numerical and experimental studies are carried out on motions of floating objects with simple geometries for instance a cylinder, representing a buoy or a floating pontoon in offshore applications, or objects with more complicated characteristics such as platforms of floating offshore wind turbines and ships. Wave-current-structure interaction of offshore structures is commonly studied by using two numerical approaches, namely the computational fluid dynamics and boundary element methods. In the former approach, the Navier-Stokes equations are solved for the entire domain and responses of the structure to linear and nonlinear waves, uniform and nonuniform current with various velocity profiles can be obtained, see for instance [1], [2], [3] and [4] among others. Computational fluid dynamics provides a relatively complete description of the environmental loadings on a floating structure; however they are computationally expensive. In the boundary element methods, it is assumed that the fluid is inviscid and incompressible, and the flow is irrotational. Thus, the viscous effect and the vortices formed at the edges of the body are not considered. Nevertheless, the boundary element methods are fast and efficient and commonly the preferred option at the design and optimization stages of a floating structure. See [5], [6], [7] and [8] on application of boundary element methods to obtain motion and hydrodynamic loads of waves only and waves and current interaction with floating structures.

As a body advances at a constant speed in regular waves, it generates a steady Kelvin pattern plus several systems of linear time-harmonic waves. In boundary element methods, an approximate description of the steady waves is obtained by means of a double body flow which is applicable in low forward speeds, see [9] and [10]. The problem is extensively studied by [11], [12], [13], [14] among others by different expressions of the Green function and/or the velocity potentials with respect to the Strouhal number, $\tau = \dfrac{|U|\,\omega_e}{g}$, where U is the forward speed, ω_e is the encounter frequency and g is the gravitational acceleration. In this study, the nonsecular expression of the Green function given by [9], at $\tau \leq 0.25$ is applied. The Green function is defined as a sum of a term representing the Green function for wave diffraction-radiation without forward speed and terms due to the forward speed and it is uniformly valid in near and far fields around the object.

Prior to hydrodynamic analysis of wave-current interaction with offshore platforms, this study focuses on a preliminary analysis on floating objects with simple geometries. Floating columns with circular and rectangular cross sections are widely applied in many offshore structures, for instance oil and gas platforms, floating substructures of offshore wind turbines and wave and current energy converters. Hence, in this study, linear wave-current interaction with circular and square cylinders is presented. The numerical results in here will be compared with laboratory measurements and numerical results by computational fluid dynamics on wave and current interaction with circular and square cylinders in future studies. Therefore, the presented numerical results are determined for scale-model dimensions. In this preliminary analysis, the motions and hydrodynamic loads on the model-scale floating cylinders are computed with boundary element method. Firstly, the responses of the freely floating cylinders to waves are computed and compared with those when the current loads are present. Next, the effect of mooring lines are studied on waves-induced motions of the cylinder and for the case when both waves and current loads are present. Finally, the motions of the cylinders to aligned and misaligned waves and current are obtained and discussed.

The interaction of a floating cylinder to waves only, and combined waves and current is studied by use of linear wave diffraction theory with a Green function for small forward speeds. Firstly, the dimensions of the object and the properties and the characteristics of the mooring lines are presented. Next, the theory and the governing equations, and the applied numerical solution on wave-current-structure interactions are discussed. Hydrodynamic loads on each cylinder and their motions due to waves, and combined waves and current, are obtained. The results for unmoored and moored cylinders are compared. Next, the effect of the incoming wave heading angle on the wave-current induced motions of both cylinders is investigated. Finally, concluding remarks about this study's analysis are provided.

2 The square and circular cylinders

The dimensions of the two cylinders, and the characteristic and properties of the mooring lines are provided in this section. The side length of the square cylinder and the diameter of the circular cylinder are 0.2 m. Both cylinders are 0.05 m thick and are submerged at $d = 0.018$ m, see Fig. 1. The mass of the circular and square cylinders are 0.5213

Copyright © 2023 by ASME

kg, 0.6615 kg and their centres of gravity are 0.007 m and 0.00703 m above the still water level (SWL), respectively.

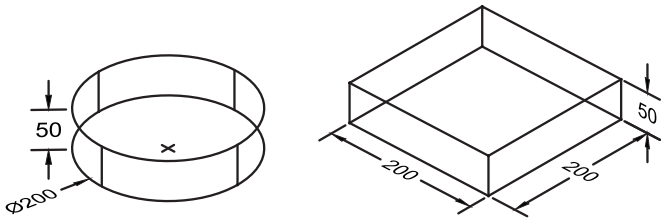

FIGURE 1. Schematic of the circular and square cylinders considered in this study. Dimensions are in mm.

In this study, both freely floating and moored cylinders are considered. If the cylinders are moored, they are connected to the seabed with catenary mooring lines, such that the lines are connected to the bottom four corners of the square cylinder and in case of the circular cylinder, the four catenary lines are connected with an angle of 22.5° with respect to the x- and y-axis of the global coordinates system. The properties of the mooring lines are the same for both circular and square cylinders and are reported in Table 1.

TABLE 1. Properties of the catenary mooring lines.

Modulus of elasticity (MPa)	1.93×10^{11}
Area of cross-section (m^2)	9×10^{-6}
Density (kg/m^3)	0.3682
Unstretched length (m)	0.325

3 Theory & numerical solution

A moving Cartesian coordinate system is chosen with its origin on the SWL and z-axis pointing upwards, see Fig. 2. The coordinate system is in steady translation with the mean forward speed of the structure or the current speed, U such that x-axis is in the same direction as the forward speed. Assuming that wave amplitude and the wave-current induced motions and rotations of the structure are small and the viscous forces are negligible, the hydrodynamic loads and the wave-current interaction with the body are obtained with linear diffraction theory. ω is the incoming wave frequency and the encounter frequency is,

$$\omega_e = \omega - |U|\, k \cos(\beta), \tag{1}$$

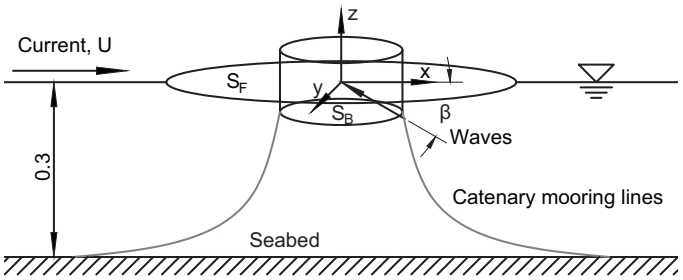

FIGURE 2. Schematic of the moored circular cylinder.

where k and β are the incoming wave number and wave heading angles, respectively.

The total velocity potential, $\Phi(x,y,z)$, equals the sum of steady velocity potential, $\bar{\phi}_s(x,y,z)$ and time harmonic velocity potentials, $\phi(x,y,z)$,

$$\Phi(x,y,z,t) = |U|\,(\bar{\phi}_s - x) + \Re\{\phi\, e^{i\omega_e t}\}. \tag{2}$$

The steady velocity potential is computed by double-body flow and satisfies the below boundary conditions on the body and the free surfaces, S_B and S_F,

$$\frac{\partial \bar{\phi}_s}{\partial z} = 0, \quad \text{on } S_F, \tag{3}$$

$$\frac{\partial \bar{\phi}_s}{\partial n} = n_x, \quad \text{on } S_B, \tag{4}$$

where n is the normal vector on the body surface, $n = (n_x, n_y, n_z)$, pointing inwards out of the fluid. Furthermore, the time-harmonic velocity potential satisfies a boundary condition at the free surface, S_F, see e.g. [10] for more details,

$$-\frac{\omega_e^2}{g}\phi + 2i\tau\frac{\partial \phi}{\partial x} + \frac{\partial \phi}{\partial z} - 2i\tau\nabla\bar{\phi}_s\nabla\phi + i\tau\phi\frac{\partial^2 \bar{\phi}_s}{\partial z^2} = 0, \quad \text{on } S_F. \tag{5}$$

Following the free surface condition, Eq. (5), the time-harmonic velocity potential can be expressed with three terms, namely the incident velocity potential and the linear velocity potential, ϕ^I and ϕ^L, and a term representing the interaction of wave radiation-diffraction with the local steady flow at the free surface, ϕ^N.

$$\phi = \phi^I + \phi^L + \tau\phi^N. \tag{6}$$

By substituting Eq. (6) into the free surface boundary condition, Eq. (5), ϕ^L and ϕ^N satisfy homogeneous and

Copyright © 2023 by ASME

non-homogeneous boundary conditions on the free surface, respectively,

$$-\frac{\omega_e^2}{g}\phi^L + 2i\tau\frac{\partial\phi^L}{\partial x} + \frac{\partial\phi^L}{\partial z} = 0, \quad \text{on } S_F, \tag{7}$$

$$-\frac{\omega_e^2}{g}\phi^N + 2i\tau\frac{\partial\phi^N}{\partial x} + \frac{\partial\phi^N}{\partial z} = Q, \quad \text{on } S_F, \tag{8}$$

where Q is defined as,

$$Q = 2\,i\nabla\bar{\phi}_s\nabla(\phi^I+\phi^L) - i(\phi^I+\phi^L)\frac{\partial^2\bar{\phi}_s}{\partial z^2}, \quad \text{on } S_F. \tag{9}$$

Moreover, both linear and nonlinear velocity potentials satisfy boundary conditions on the wetted surface of the body in radiation and diffractions problems. The boundary conditions of ϕ^L and ϕ^N on the body surface for the diffraction problem are,

$$\frac{\partial\phi^L}{\partial n} = -\frac{\partial\phi^I}{\partial n}, \qquad \frac{\partial\phi^N}{\partial n} = 0, \quad \text{on } S_B, \tag{10}$$

and the boundary conditions of ϕ^L and ϕ^N on the body surface for the radiation problem are,

$$\frac{\partial\phi^L}{\partial n} = n_j, \qquad \frac{\partial\phi^N}{\partial n} = \frac{i\,m_j}{k}, \quad \text{on } S_B, \tag{11}$$

where m_j terms are defined by double derivatives of the local steady velocity potential, see [10] for more details on its formulations.

The Green function for nonzero forward speed

Assuming that the current speed is small, *i.e.* $\tau \leq 0.25$, the Green function given by Noblesse & Chen (1995), [9] is used to study wave-current effect on a floating body with arbitrary shape. The Green function is expressed as the sum of the Green function for wave radiation-diffraction problems and a term that is a function of the incoming current speed,

$$4\,\pi\,G = G^R + G^H, \tag{12}$$

where, G^R and G^H are the singular and regular terms of the Green function,

$$G^R = -\frac{1}{r} - \Big(\frac{2e^{i\,\tau X}-1}{r'}\Big), \tag{13}$$

$$G^H = -2e^{i\,2\,\tau X}\Big(G_0 + i\,2\tau(\frac{X}{H})\,(1+Z)\,G_1\Big). \tag{14}$$

In Eqs. 12 and 13, (x,y,z) and (ξ,η,ζ) are the source and field point coordinates, and r and r' are $r = \sqrt{(\xi-x)^2+(\eta-y)^2+(\zeta-z)^2}$ and $r' = \sqrt{(\xi-x)^2+(\eta-y)^2+(\zeta+z)^2}$, respectively. Furthermore, $(X,Y,Z) = k = (\xi-x, \eta-y, \zeta-z)$, $H = \sqrt{X^2+Y^2}$, and G_1 and G_2 are the regular part of the Green function for wave radiation-diffraction problem without forward speed and its derivatives with respect to H,

$$G_1 = \pi\Big[\tilde{E}_0(H) + iJ_0(H)\Big]e^Z + N_0(H,Z), \tag{15}$$

$$G_2 = \pi\Big[\tilde{E}_1(H) + iJ_1(H)\Big]e^Z + N_1(H,Z), \tag{16}$$

where $J_0(H)$, $J_1(H)$ and $\tilde{E}_0(H)$ and $\tilde{E}_1(H)$ are the Bessel and Weber functions, see [15]. Furthermore, $N_0(H,Z)$ and $N_1(H,Z)$ are defined in [16] and [17].

Wave forces and moments

The first order dynamic pressure, p, is obtained by Euler's integral,

$$\begin{aligned} p = -\rho\Big(&g\,z - i\,\omega_e\,(\phi^I+\phi^L+\tau\phi^N) + \\ &U\,\nabla\,(\bar{\phi}_s - x)\,\nabla(\phi^I+\phi^L)\Big). \end{aligned} \tag{17}$$

Following Eq. (17), the first order excitation forces and moments are computed as,

$$\begin{aligned} F_j^{exc} = -i\,\rho\,\omega_e &\iint_{S_B}(\phi_j^I+\phi_j^L+\tau\phi_j^N)\,n_j\,dS + \\ &\frac{\rho\,g}{\omega_e}\iint_{S_B}\nabla\,(\bar{\phi}_s - x)\,\nabla(\phi_j^I+\phi_j^L)n_j\,dS. \end{aligned} \tag{18}$$

Similarly, the added mass and damping coefficients, a_{jk} and b_{jk}, respectively, are obtained,

Copyright © 2023 by ASME

$$R_{jk} = -i\rho\omega_e^2 \iint_{S_B} (\phi_{jk}^L + \tau\phi_{jk}^N)\, n_k\, dS - i\rho\, g \iint_{S_B} \nabla(\bar{\phi}_s - x)\, \nabla(\phi_{jk}^L)\, n_k\, dS, \tag{19}$$

where,

$$a_{jk} = \Re\Big\{\frac{1}{\omega_e^2} R_{jk}\Big\}, \qquad b_{jk} = \Im\Big\{\frac{1}{\omega_e} R_{jk}\Big\}. \tag{20}$$

Equation of motion

Assuming $\tau \leq 0.25$, the equation of motion of a floating structure to waves and current is obtained by,

$$\xi_k \Big(-\omega_e^2 (M_{jk} + a_{jk}) + i\omega_e b_{jk} + c_{jk,\text{hst}} + c_{jk,\text{moor}}\Big) = A F_j^{exc}, \quad j,k = 1,2,\cdots,6, \tag{21}$$

where A is the wave amplitude and $c_{jk,\text{hst}}$ and $c_{jk,\text{moor}}$ are the hydrostatic and mooring lines stiffness coefficients, receptively. ξ_k is the complex body response phasor in mode k and M_{jk} is the linearised body inertia mass matrix. The response amplitude operators (RAOs) of the structure to waves and current for $\tau \leq 0.25$, $|\frac{\xi_k}{A}|$, are obtained by solving Eq. (21) at encounter frequency ω_e.

Numerical solution

The numerical solution of the wave-current-structure interaction is obtained in HYDRAN-XR (see [18]), a potential flow solver for hydrodynamic analysis integrated with finite element method for structural considerations. HYDRAN-XR is modified and the nonsecular Green function for small forward speed, given by Noblesse et al. (1995), [9] is implemented.

Panel mesh over the wetted surface of the body, S_B and on the free surface at the vicinity of the object, S_F are generated. HYDRAN-XR solves the diffraction and radiation problem over S_B and the double body flow over S_F by boundary integral equations with a three dimensional source distribution, Green function method, see e.g. [19].

4 Results & discussion

In this section, waves and wave-current interaction with the square and circular cylinders are studied. First, the excitation force in surge and the excitation moment in pitch on the cylinders for wave loads and combined waves and current are computed and compared. Next, motions of the freely floating circular and square cylinders to waves, and combined waves and current loads are computed and compared with those when the mooring lines are present. Furthermore, the effect of waves and current misalignment on the motions of the moored cylinders is investigated.

The simulations are carried out for three wave heading angles, $\beta = 0^\circ$, 30° and 45°, and wave periods 0.5 s to 2 s, considering the dimensions of the cylinders. Furthermore, the current speed is 0.06 m/s. Body mesh convergence studies are performed for both cylinders with panel lengths 0.005 m, 0.008 m and 0.02 m as fine, medium and coarse meshes. Results of medium and fine meshes of the cylinders were converged. The free surface panel mesh covers an area with its radius equal to five times the diameter of the cylinders. The free surface mesh with maximum panel size of 0.01 m is with 46368 and 50560 panels for square and circular cylinders, respectively. The medium mesh of the square and circular cylinders were 925 and 1440 panels and their simulations take approximately 1 hour and 45 minutes, and 1 hour, respectively on a desktop machine with Intel Core *i*5 8600, 3.10 G*hz* CPU and 32 GB memory.

Excitation forces and moments

Figure 3 shows the excitation force in surge, F_1^{exc}, and the excitation moment in pitch, M_5^{exc}, on the circular and square cylinders for two load cases, waves only and combined waves and current. In general, the square cylinder experiences slightly larger excitation force and moment compared with the circular cylinder. Furthermore, F_1^{exc} and M_5^{exc} on the circular and square cylinders increase when both waves and current are present.

Freely floating cylinders

Figure 4 shows the wave- and combined waves and current-induced motions of the freely floating circular and square cylinders in surge, heave and pitch with respect to encounter wave periods. Since the floating cylinders are in model-scale dimensions, the pitch RAOs are given in deg/mm. Larger surge RAOs are observed from freely floating cylinders when only waves are present compared with those due to combined waves and current effect. However, both heave and pitch RAOs increase when the current

Copyright © 2023 by ASME

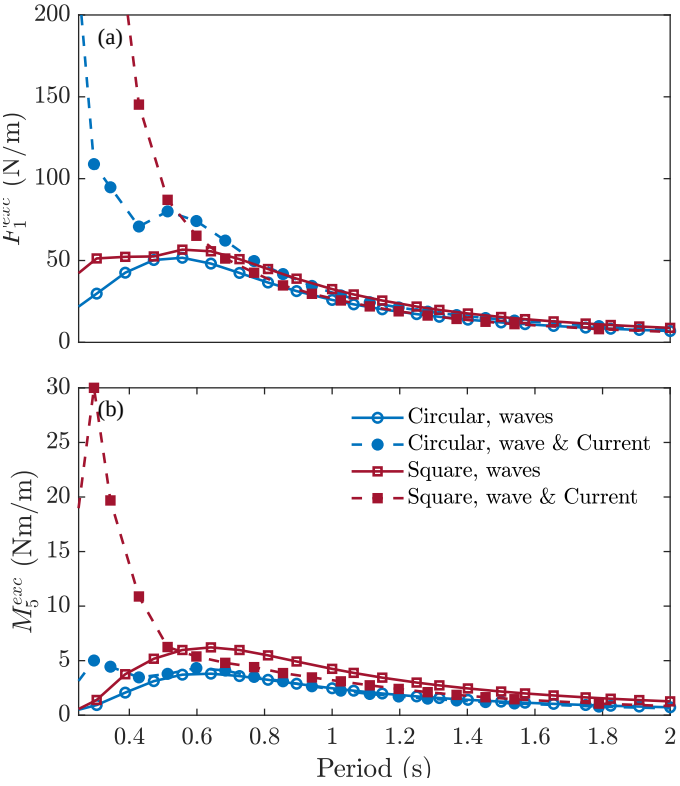

FIGURE 3. Comparison of (a) the excitation force in surge and (b) excitation moment in pitch on circular and square cylinders to waves, and combined waves and current loads.

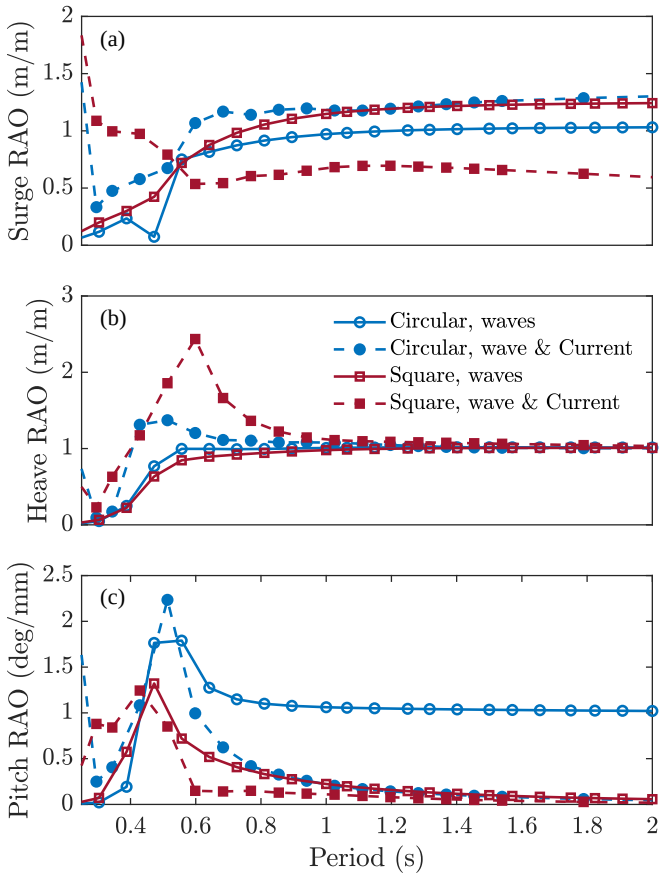

FIGURE 4. Comparison of (a) surge, (b) heave and (c) pitch responses of the freely floating circular and square cylinders to waves, and combined waves and current loads.

is added. Pitch RAOs of both cylinders experience a peak at 0.5 s, approximately the natural period of the floating cylinders in pitch.

Moored cylinders

Next, the circular and square cylinders are connected to the seabed with four catenary mooring lines. The properties and the characteristics of the mooring lines are given in table 1. RAOs of both moored cylinders to waves are compared with those to waves and current loads in Fig. 5. Similar to Fig. 4, surge motions of the cylinders decrease when current loads are added whereas the heave and pitch RAOs to waves and current are larger than those to wave loads only. Furthermore, pitch RAOs of the circular cylinders decrease significantly when the mooring lines are added compared with those of the freely floating circular cylinder, shown in Fig. 4. Nonetheless, the square cylinder undergoes large pitch motions with mooring lines added, to both waves only and waves and current loads.

Waves and current misalignment

In this section, motions of the circular and square cylinders to co-directional waves and current are computed and compared with those when the waves and current are misaligned. In this study, the current direction is always parallel with the x-axis of the global coordinate system, but the wave heading angle changes from $\beta = 0^\circ$ to $\beta = 30^\circ$ and 45°. Surge, heave and pitch RAOs of the circular and square cylinders for the three wave heading angles are computed and compared.

Figure 6 and 7 show the comparison of the RAOs of the moored circular and square cylinders to co-directional and misaligned waves and current, *i.e.* $\beta = 30^\circ$ and 45°. It can be seen that surge and pitch motions of both cylinders decrease as the angle between the incoming waves and current increases from $\beta = 0^\circ$ to $\beta = 45^\circ$. Furthermore, the effect of β on the heave motions of the cylinders is negligible.

Copyright © 2023 by ASME

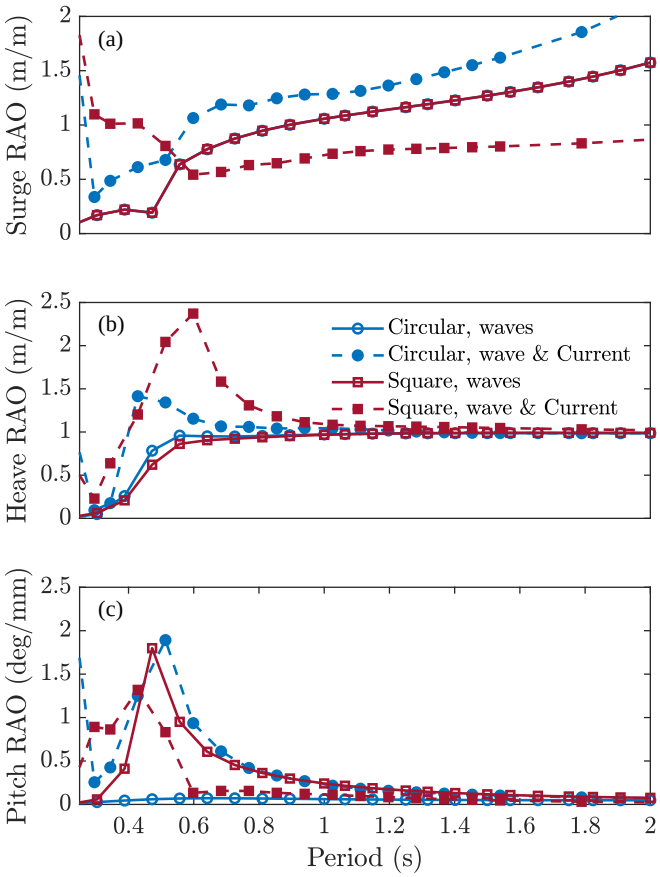

FIGURE 5. Comparison of (a) surge, (b) heave and (c) pitch responses of the moored circular and square cylinders to waves, and combined waves and current loads.

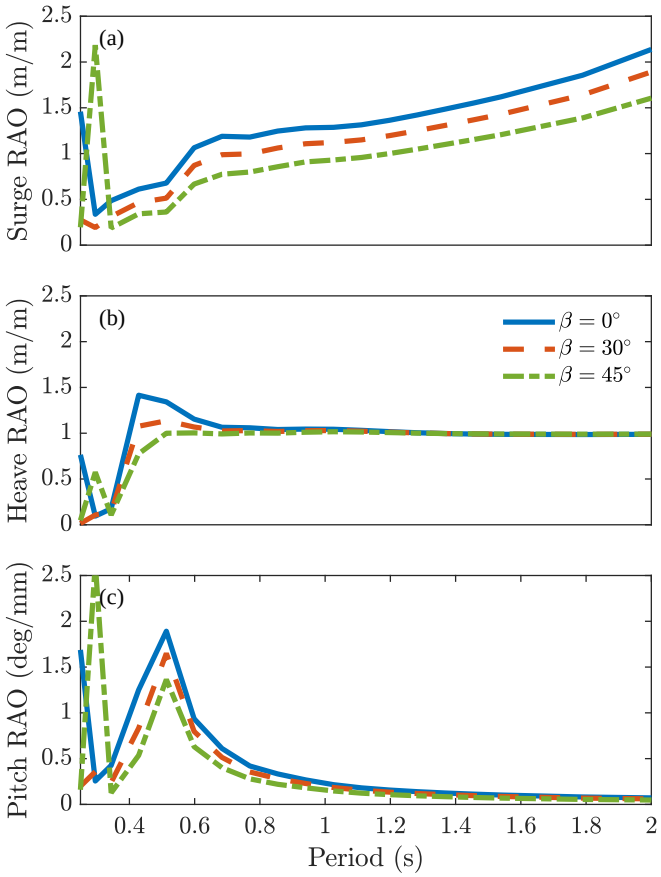

FIGURE 6. Comparison of (a) surge, (b) heave and (c) pitch responses of the moored circular cylinder to aligned and misaligned waves and current loads, at $\beta = 0°$, 30° and 45°.

5 Concluding Remarks

Wave-current interactions of two cylinders with square and circular cross sections are studied by use of the boundary element method with a Green function for small forward speed. The waves- and combined waves and current-induced excitation forces on both cylinders in surge and the moments in pitch are computed and compared. Commonly, the addition of the current that is co-directional with the incoming waves results in larger excitation force in surge and excitation moment in pitch. The motion of the cylinders are obtained for waves only and are compared with those when both waves and current interact with the cylinders. Furthermore, for both load cases, the effect of catenary mooring lines on the motions of the circular and square cylinders is studied. It is seen that when the current loads are added the surge motions of the cylinders decrease slightly compared with their wave-induced surge motions. However, both heave and pitch RAOs to waves and current are larger than those due to waves loads. Finally, the effect of waves and current misalignment on the motions of the cylinders is studied.

Addition of current loads and mooring lines results in different responses of the floating cylinders compared with when only wave loads are present. This study emphasises the importance of considering the wave-current interaction for a better description of the environmental loads on offshore structures.

REFERENCES

[1] Di Paolo, B., Lara, J. L., Barajas, G., Paci, A., and Losada, I. J., 2018. "Numerical analysis of wave and current interaction with moored floating bodies using overset method". In Volume 2: CFD and FSI, June 17-22, Madrid, Spain, American Society of Mechanical Engineers, pp. 1–10, doi:10.1115/OMAE2018–77284.

[2] Fang, Y., Yang, Z., Ma, Y., and Li, Q., 2020. "Study of flow through and around a square cylinder array". *Journal of Physics: Conference Series,* ***1600***(1),

Copyright © 2023 by ASME

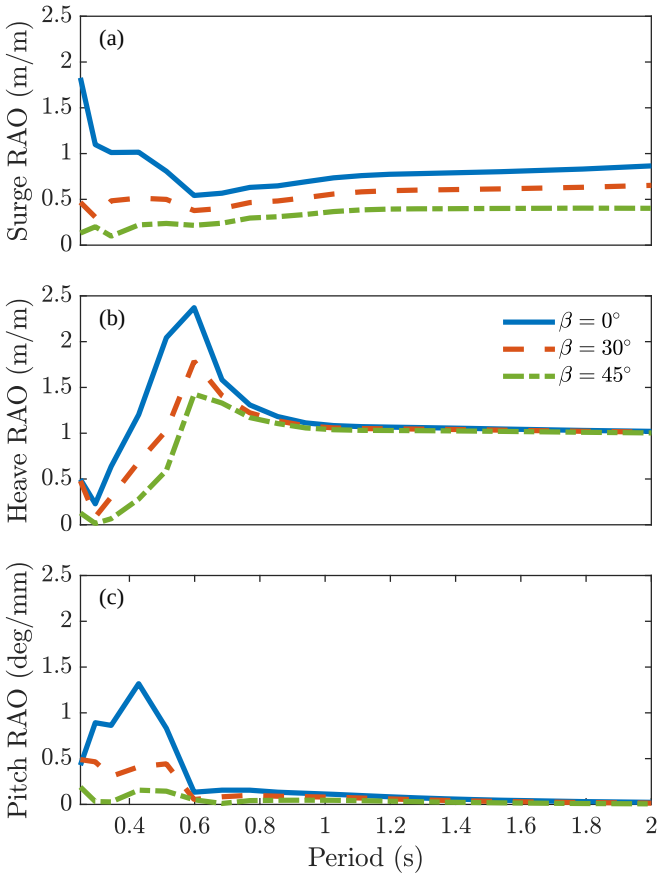

FIGURE 7. Comparison of (a) surge, (b) heave and (c) pitch responses of the moored square cylinder to aligned and misaligned waves and current loads, at $\beta = 0°$, $30°$ and $45°$.

pp. 1–9, doi:10.1088/1742–6596/1600/1/012029.

[3] Kim, S. J., and Kim, M. H., 2022. "The nonlinear wave and current effects on fixed and floating bodies by a three-dimensional fully-nonlinear numerical wave tank". *Ocean Engineering,* ***245***, pp. 1–15, doi:10.1016/j.oceaneng.2021.110458.

[4] Lamei, A., Hayatdavoodi, M., and Moir, S., 2022. "Power production from a hydrokinetic device: Mass of water turbine". In ASME 41st International Conference on Ocean, Offshore, and Arctic Engineering, June 5-10, Hamburg, Germany, ASME, pp. 1–10.

[5] Monroy, C., Giorgiutti, Y., and Chen, X.-B., 2012. "First and Second Order Wave-Current Interactions for Floating Bodies". In Volume 1: Offshore Technology, July 1-6, 2012, Rio de Janeiro, Brazil, Vol. 1, American Society of Mechanical Engineers, pp. 373–382, doi:10.1115/OMAE2012–83409.

[6] Lalli, F., Bruschi, A., Liberti, L., Pesarino, V., and Bassanini, P., 2012. "Analysis of linear and nonlinear features of a flat plate breakwater with the boundary element method". *Journal of Fluids and Structures,* ***32***, pp. 146–158, doi:10.1016/j.jfluidstructs.2012.01.009.

[7] Lamei, A., Hayatdavoodi, M., and Riggs, H. R., 2022. "Motion and elastic response of wind-tracing floating offshore wind turbines". *Journal of Ocean Engineering and Marine Energy*, pp. 1–25, doi:10.1007/s40722–022–00250–1.

[8] Lamei, A., Hayatdavoodi, M., and Riggs, H. R., 2022. "Hydroelastic response of wind-tracing floating offshore structures to irregular waves andwind". In 9th International Conference on hydroelasticity in marine technology, June 10–13, Rome, Italy.

[9] Noblesse, F., Taylor, D., and Chen, X. B., 1995. "Decomposition of free-surface effects into wave and near-field components". *Ship Technology Research,* ***42***(4), pp. 167–185.

[10] Chen, X. B., and Malenica, Š., 1998. "Interaction effects of local steady flow on wave diffraction-radiation at low forward speed". *International Journal of Offshore and Polar Engineering,* ***8***(2), pp. 101–109.

[11] Zhao, R., and Faltinsen, O., 1988. "Wave-current interaction effects on large-volume structures". In Conference on Behaviour of Offshore Structures, June, Trondheim, Norway, no. 1, pp. 187–190.

[12] Taylor, R. E., 1990. "The hydrodynamic force on an oscillating ship with low forward speed". *Journal of Fluid Mechanics,* ***211***(333), pp. 333–353, doi:10.1017/S0022112090001598.

[13] Nossen, J., Grue, J., and Palm, E., 1991. "Wave forces on three-dimensional floating bodies with small forward speed". *Journal of Fluid Mechanics,* ***227***, pp. 135–160, doi:10.1017/S002211209100006X.

[14] Grue, J., and Biberg, D., 1993. "Wave forces on marine structures with small speed in water of restricted depth". *Applied Ocean Research,* ***15***(3), jan, pp. 121–135, doi:10.1016/0141–1187(93)90036–W.

[15] Abramowitz, M., 1974. *Handbook of Mathematical Functions, With Formulas, Graphs, and Mathematical Tables,*. Dover Publications, Inc., USA.

[16] Telste, J. G., and Noblesse, F., 1986. "Numerical evaluation of the green function of water-wave radiation and diffraction". *Journal of Ship Research,* ***30***(02), jun, pp. 69–84, doi:10.5957/jsr.1986.30.2.69.

[17] Ponizy, B., Noblesse, F., Ba, M., and Guilbaud, M., 1994. "Numerical evaluation of free-surface green functions". *Journal of Ship Research,* ***38***(03), sep, pp. 193–202, doi:10.5957/jsr.1994.38.3.193.

Copyright © 2023 by ASME

[18] NumSoft Technologies, 2020. Hydran-xr, hydrodynamic response analysis with integrated structural finite element analysis, version 20.1. Tech. rep., Numsoft Technologies.

[19] Ertekin, R. C., Riggs, H. R., Che, X. L., and Du, S. X., 1993. "Efficient methods for hydroelastic analysis of very large floating structures". *Journal of Ship Research,* ***37***(1), pp. 58–76, 10.5957/jsr.1993.37.1.58.

Copyright © 2023 by ASME